

THEORETICAL ANALYSIS AND NUMERICAL MODELLING OF PORTEVIN–LE CHÂTELIER DEFORMATION BANDS

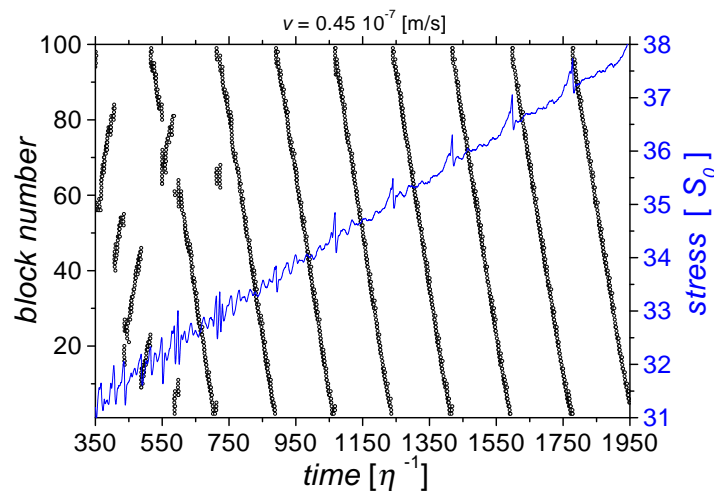
E. RIZZI^{1,*}, P. HÄHNER^{2,*}

¹ *Dipartimento di Ingegneria Civile e Ambientale, Facoltà di Ingegneria di Taranto, Politecnico di Bari, rizzi@stru.polimi.it*

² *Institute for Advanced Materials, European Commission, Joint Research Center, Petten, The Netherlands, hahner@jrc.nl*

**Work performed at IMNF, Technische Universität Braunschweig, Germany*

Plastic instabilities associated to the Portevin–Le Châtelier (PLC) effect represent an instructive example of anomalous plastic deformation in metal alloys. The understanding of this behaviour necessitates bridging different scales: while *microscopic* interactions between glide dislocations and solute atoms (Dynamic Strain Ageing, DSA) and *mesoscopic* dislocation–dislocation interactions (correlated dislocation motion) give rise to plastic instability, the effect manifests itself by *macroscopic* inhomogeneity of plastic flow (deformation banding). The spatio-temporal dynamics of PLC deformation bands is investigated with a model which incorporates an explicit physical description of the DSA kinetics. PLC deformation banding is traced back to a wave propagation phenomenon, and problems regarding spatial coupling and propagation velocity selection are addressed. Analytical predictions referring to solitary deformation bands, as well as the relevant band parameters (propagation velocity, localized strain and band width) are derived. The theoretical analysis is validated by numerical simulations which display features in good qualitative agreement with theory and with experimental observations of the PLC effect in aluminium alloys. They include the appearance of the various types of PLC bands ranging from solitary Type A, to intermittent Type B and to random Type C.



Simulated tensile test at constant cross-head velocity v ($\eta=0.1 \text{ s}^{-1}$, $S_0=1 \text{ MPa}$): space–time localization map and corresponding stress–time curve in a time window showing Type C and Type B PLC bands.

THEORETICAL ANALYSIS AND NUMERICAL MODELLING OF PORTEVIN–LE CHÂTELIER DEFORMATION BANDS

E. RIZZI^{1,*}, P. HÄHNER^{2,*}

¹*Dip. di Ingegneria Civile e Ambientale, Facoltà di Ing. di Taranto, Politecnico di Bari*

²*Institute for Advanced Materials, European Commission, JRC Petten, The Netherlands*

** Work performed at IMNF, Technische Universität Braunschweig, Germany*

SOMMARIO

In questa nota si presenta un modello analitico-numerico del fenomeno di instabilità plastica in soluzioni metalliche solide usualmente noto come effetto Portevin-Le Châtelier.

ABSTRACT

This paper presents an analytical-numerical model of the plastic instability phenomenon in metallic solid solutions usually referred to as Portevin-Le Châtelier effect.

1. INTRODUCTION

Plastic flow of metallic alloys subjected to various deformation conditions may display oscillatory behaviour. Under constant applied stress rate the typical stress–strain trace is wavy (staircase type), while under constant applied strain rate, the stress profile is serrated (saw-tooth type). This irregular plastic flow is a form of material instability and associated inhomogeneous deformation (strain localization), which is referred to as Savart–Masson or, more commonly, as Portevin–Le Châtelier (PLC) effect, see e.g. [1, 3, 7]. The PLC effect is primary known to arise from Dynamic Strain Ageing (DSA), that is the dynamic interaction between gliding dislocations and mobile solute atoms, see e.g. [2]. The local DSA processes may induce a negative Strain Rate Sensitivity (SRS) of the flow stress, namely a decrease of the flow stress with an increasing applied strain rate and result in macroscopic plastic oscillations. As opposed to inhomogeneous plastic yield phenomena due to *strain-softening* (Lüders bands), that may be handled by appropriate pre-deformation, the unstable plastic flow due to *strain-rate-softening* (PLC bands) is repetitive and the PLC range needs to be avoided in the industrial processes (e.g. sheet forming in automotive industry). Different types of PLC instabilities can be observed depending on the spatio-temporal organization of the deformation bands. Type C bands

appear almost at random in the sample without propagating, Type B bands exhibit an oscillatory or intermittent propagation, and Type A bands propagate continuously as solitary plastic waves. Correspondingly, the stress–strain curves display regular equidistant stress drops for Type A bands, heavily serrated flow for Type C bands, and a superposition of the two profiles for Type B bands.

Recently the present authors have proposed a new model of the PLC effect that attempts to bridge the microstructural aspects of DSA with the macroscopic mechanical behaviour associated with the PLC instabilities [4, 5, 6]. The model is coupled in time and (one-dimensional) space and introduces two intrinsic time scales in the evolution equations and a characteristic length scale through a diffusion-like term with spatial second-order gradient. The main constitutive equations and analytical derivations of such model are first summarized in the present work. Then, new numerical simulations of the model are presented, in particular regarding the application of discontinuous strain rate jumps within the PLC range, or from outside to inside the PLC range, or conversely. The numerical results display the same rich qualitative patterns of strain localization and corresponding phenomenological stress–strain responses in agreement with [6]. The band kinematics characteristics of Type A PLC bands are also consistent with systematic numerical simulations provided in [5]. These numerical simulations display very good qualitative agreement with the experimental observation of the PLC effect in metal alloys.

2. MODEL EQUATIONS AND ANALYTICAL RESULTS

The present model of the PLC effect is based on the following evolution equations for the *plastic* strain rate $\varepsilon_{,t}$ and the rate $(\Delta G)_{,t}$ of the additional activation enthalpy ΔG linked to DSA (see [4, 5]):

$$\begin{cases} \varepsilon_{,t} &= \nu \Omega \exp \left[-\frac{G_0 + \Delta G}{kT} + \frac{\sigma_{\text{ext}} - \sigma_{\text{int}}}{S_0} \right], \\ (\Delta G)_{,t} &= D \Delta G_{,xx} + \eta (\Delta G_\infty - \Delta G) - \frac{\varepsilon_{,t}}{\Omega} \Delta G. \end{cases} \quad (1)$$

The first Arrhenius-type equation (1)_a interprets plastic flow as a thermally-activated process of dislocation motion. Ω and ν are physical parameters representing the elementary plastic strain corresponding to the activation of all mobile dislocations and the attempt frequency of thermal activation; $k=1.38 \cdot 10^{-23}$ J/K is the Boltzmann constant and T the (constant) absolute temperature; $G=G_0+\Delta G$ is the Gibbs free activation enthalpy, with G_0 the constant activation enthalpy in the absence of DSA; $\sigma_{\text{eff}}(\varepsilon, \varepsilon_{,t}, \Delta G)=\sigma_{\text{ext}}(\varepsilon, \varepsilon_{,t}, \Delta G)-\sigma_{\text{int}}(\varepsilon)$ is the effective stress available to propel dislocation motion, namely the difference between the externally applied stress σ_{ext} (flow stress) and the internal stress σ_{int} (back stress) resulting from other defects and linked to plastic strain hardening (quasi-linear strain hardening is assumed, $\sigma_{\text{int},t}=h \varepsilon_{,t}$, with h a constant piece-wise linear hardening parameter); S_0 is the (positive) *instantaneous* SRS of the flow stress $S_0=\partial \sigma_{\text{ext}}/\partial \ln \varepsilon_{,t}|_{\varepsilon, \Delta G}$, which is generally distinct from the *asymptotic* SRS S_∞ of the model $S_\infty=\partial \sigma_{\text{ext}}/\partial \ln \varepsilon_{,t}|_{\varepsilon}$ (see [7]), that may become negative in the PLC range.

The three terms in the second evolution equation (1)_b interpret respectively the following phenomena: long-range dislocation interaction (diffusion-like coupling based on spatial second-order gradient), ageing linked to dislocations pinning by the solute atoms,

dislocations unpinning by thermal activation and release of the solute cloud. D is the diffusion coefficient, with dimensions of $[L]^2/[t]$; ΔG_∞ is the maximum value of the additional activation enthalpy that can be induced by DSA; η^{-1} is the intrinsic time scale of the ageing process, which competes with the time scale $\Omega/\varepsilon_{,t}$ linked to thermal activation.

To account for a spatially-extended system, the constitutive equations (1) must be complemented by the ‘*machine equation*’ $\sigma_{\text{ext},t}/E_{\text{eff}}=v/l-1/l \int_0^l \varepsilon_{,t} dx$, which expresses the additive composition of elastic and plastic deformation rates to comply with the imposed cross-head velocity v . Here $E_{\text{eff}}=E E_m/(E + E_m)$ is the effective elastic stiffness of the system composed of the specimen (Young’s modulus E) and the tensile machine (elastic modulus E_m), and l is the parallel length of the specimen.

To simplify the model equations and reduce the number of independent parameters, the PLC model (1) is better expressed in terms of non-dimensional variables:

$$\begin{cases} \dot{f} = \dot{\sigma} f - \theta \exp[-g] f^2, & (2) \\ \dot{g} = g'' + g_\infty - g - f \exp[-g] g. & (3) \end{cases}$$

Here f is the non-dimensional driving force linked to the effective stress, $f \equiv f_0 \exp[\sigma_{\text{eff}}/S_0]$, $f_0 \equiv \nu/\eta \exp[-G_0/(kT)]$, while g is the non-dimensional additional activation enthalpy $g \equiv \Delta G/(kT)$. Accordingly, $g_0 \equiv G_0/(kT)$ and $g_\infty \equiv \Delta G_\infty/(kT)$. The overscored dot denotes the derivative with respect to the non-dimensional time $\tilde{t} = \eta t$, namely $(\dot{}) = ()_{,t}/\eta$. The dimensionless stress rate $\dot{\sigma}$ and hardening coefficient θ are scaled parameters which relate to the actual stress rate $\sigma_{\text{ext},t}$ and the strain hardening coefficient h as $\dot{\sigma} = \sigma_{\text{ext},t}/(\eta S_0)$, $\theta = \Omega h/S_0$. The primes in g'' denote instead differentiation with respect to the non-dimensional spatial coordinate $\tilde{x} = \sqrt{\eta/D} x$, where $\sqrt{D/\eta}$ is a characteristic length.

The non-dimensional hardening coefficient θ is assumed to be small: $\theta \ll 1$ (‘*weak hardening*’). In such case, variable f can be considered as the ‘slow’ variable of the model, whereas g represents its ‘fast’ variable. The qualitative response of the constitutive model is based on a limit cycle behavior: the system orbits around the ‘*working point*’ representing the steady state values of both variables f and g . Fast variable g oscillates rapidly at almost constant f between the minimum and maximum values g_{min} , g_{max} that may be estimated according to a ‘switching curve approximation’, see [4, 6]. The ‘working point’ must be taken on the (inaccessible) ascending branch of the adiabatic $\dot{g}=0$ characteristic. Provided that $g_\infty > 4$, such curve is ‘*N-shaped*’ and the asymptotic SRS of the model becomes negative for the plastic strain rate range

$$g_\infty - 2 - \sqrt{g_\infty(g_\infty - 4)} < 2 \varepsilon_{,t}/(\eta \Omega) < g_\infty - 2 + \sqrt{g_\infty(g_\infty - 4)}. \quad (4)$$

A linear stability analysis signals the onset of diverging perturbations around the steady state (‘*Hopf bifurcation*’) and provides the range of plastic strain rates entering the PLC regime:

$$g_\infty - 2 - \theta - \sqrt{(g_\infty - \theta)^2 - 4g_\infty} < 2(1 + \theta) \varepsilon_{,t}/(\eta \Omega) < g_\infty - 2 - \theta + \sqrt{(g_\infty - \theta)^2 - 4g_\infty}. \quad (5)$$

The PLC range is somehow narrower than that of the negative asymptotic SRS (4). This means that plastic instability develops only for some finite negative value of S_∞ . However, for weak hardening the two ranges almost coincide, since corrections of the order of $\theta \ll 1$ can be neglected.

To estimate the kinematics characteristics of solitary plastic waves (Type A PLC bands), the band plastic strain $\Delta \varepsilon_b$ can be considered to accommodate virtually the

whole applied strain rate v/l . Then, relations $v=\Delta\varepsilon_b c_b$ and $v=\varepsilon_{b,t} w_b$ link the applied cross-head velocity v to the propagation speed c_b , the local plastic strain rate in the band $\varepsilon_{b,t}$ and the band width w_b . Then, out of the three band characteristics c_b , w_b , $\Delta\varepsilon_b$, only two are independent. For the limiting case $\theta\ll 1$ the following set of band parameters can be derived based on few simplifying assumptions, [4, 6]:

$$c_b = \left(\frac{D}{\eta}\right)^{1/4} \frac{\sqrt{(1+g_{\min})/2}}{g_{\max}-g_{\min}} \sqrt{\theta} \frac{v}{\Omega\sqrt{w_b}}, \quad w_b = 2\sqrt{\frac{D}{\eta}} + \frac{g_{\min}}{g_{\infty}-g_{\min}} \frac{v}{\eta\Omega}, \quad \Delta\varepsilon_b = \frac{v}{c_b}. \quad (6)$$

Notice that the band speed c_b depends non-linearly on the applied cross-head velocity v , through eqn (6). Moreover, eqn (6) predicts a square root dependence of c_b on the non-dimensional hardening coefficient θ . The faster the material hardens, the higher is the band speed, while inversely the lower is the plastic strain carried by the band.

3. NUMERICAL RESULTS

Systematic numerical simulations of the present PLC model have been performed in [5, 6]. Here further numerical results are reported, specifically for simulated tests with a jump of the applied strain rate within the PLC range, from inside to outside the PLC range, or viceversa. The adopted model parameters are the following: $\eta=0.1 \text{ s}^{-1}$, $\Omega=10^{-5}$, $S_0=1 \text{ MPa}$, $E_{\text{material}}=E_{\text{machine}}=10^5 \text{ MPa}$ ($E_{\text{eff}}=0.5 \cdot 10^5 \text{ MPa}$), $f_{(0)}=f_0=10^{-13}$, $g_{(0)}=g_{\infty}=6$, $D=10^{-7} \text{ m}^2/\text{s}$, $l=0.1 \text{ m}$. Parabolic plastic strain hardening is prescribed by a non-dimensional hardening coefficient decreasing with the space-average plastic strain ε_{av} according to the linear dependence $\theta=\theta_0-2 \cdot 10^{-6} \varepsilon_{av}$, where $\theta_0=\Omega h_0/S_0=10^{-2}$ is the initial non-dimensional hardening coefficient corresponding to $h_0=10^3 \text{ MPa}$. The governing equations are discretized both in time and in space and solved through a Finite Differences integration scheme on the space coordinate at each discrete time instant. A non-dimensional time step $\Delta\tilde{t}=0.1$ and a density of 100 point locations ('blocks') along the specimen length have been considered. Fixed boundary conditions have been assumed, namely, for the first and last blocks, $\dot{f}=\dot{g}=0$ at each discrete time instant. To trigger the PLC instability, the initial condition $f_{(0)}$ is perturbed at certain space locations by a random multiplicative factor varying between 1 and 30, which alters locally the yield strength up to a maximum of about 10%.

We report first the results concerning Type C and Type B PLC bands for an applied strain rate of $v=0.45 \cdot 10^{-7} \text{ m/s}$ near the lower bound of the PLC range. Fig. 1 represents the space-time localization map of the plastic strain rate together with the corresponding stress-time curve in a time range near the beginning of the loading history. The PLC instability is triggered here by a random initial perturbation at all block locations. Furthermore, an additional random kick is given at each time step at a random spatial location. Type C isolated bursts of plastic activity rapidly tend to coalesce and correlate in time and space giving rise to a true Type B propagation mode.

Next, a series of tests with a sudden jump in the applied cross-head velocities is considered. Fig. 2 shows the space-time localization map and the stress-time curve for a simulated test at constant applied cross-head velocity in the PLC range jumping from $v_0=0.60 \cdot 10^{-7} \text{ m/s}$ to $v=3e v_0=4.89 \cdot 10^{-7} \text{ m/s}$. The example is instructive since it shows the sudden shift to a multiple band propagation that is typical for the higher strain

rates. These modes are associated to a characteristic wavy profile of the flow stress as it can be noticed from the stress trace near the end of the loading history.

Figs. 3, 5 and 4, 6 report respectively the simulations for a sudden jump of the strain rate from outside to inside the PLC range (from $v_0=0.20 \cdot 10^{-7}$ m/s to $v=4e v_0=2.17 \cdot 10^{-7}$ m/s) and viceversa (from $v_0=1.50 \cdot 10^{-7}$ m/s to $v=2e v_0=8.15 \cdot 10^{-7}$ m/s). Fig. 3 shows that, despite the initial random perturbations at all blocks, the initial response of the system is stable (no oscillations). At the strain rate jump, the system shifts to an unstable behavior with a reach pattern of PLC bands. As shown by the zoom view of the stress–strain curve at the strain rate jump (Fig. 5), the system responds instantaneously with the positive SRS S_0 , while then develops a negative asymptotic SRS S_∞ as it can be observed from the extrapolated stress–strain curve (see [7]). Reverse trends are observed for the opposite case. Fig. 4 shows a sharp arrest of the PLC bands and a transition into homogeneous plastic flow. Accordingly, the zoom window in Fig. 6 shows a positive asymptotic SRS S_∞ preventing the PLC effect.

Finally, a strain rate jump is considered in the PLC range of a Type A propagation example triggered by an initial perturbation at the second block only (Figs. 7-10). Fig. 7 displays a smooth reflective propagation pattern even across the strain rate jump (from $v_0=0.50 \cdot 10^{-7}$ m/s to $v=2 v_0=1.00 \cdot 10^{-7}$ m/s). The flow stress shows the typical staircase profile associated to Type A PLC bands. The band kinematics characteristics are filtered-out automatically from the plastic strain rate and plastic strain maps and represented in Figs. 8-10 as a function of the imposed hardening coefficient θ . Fig. 8 shows that the band speed c_b decreases at decreasing hardening in agreement with the square root dependence estimated in eqn (6). The band speed ranges from about 0.04 to 0.09 blocks per second, namely, with the assumed length $l=0.1$ m and 100 blocks, between 0.04 and 0.09 mm/s. The band width (Fig. 9) is practically constant according to the approximate evaluation of eqn (6) and displays a jump from about 9 blocks (mm) to about 14 blocks (mm). Finally, the plastic strain $\Delta\varepsilon_b$ carried by the band (Fig. 10) also jumps and shows a converse $1/\sqrt{\theta}$ dependence according to eqn (6) while ranging smoothly from about 0.06 to 0.22%. These results on the band characteristics agree well with the theoretical prediction and with the previous systematic numerical simulations in [5].

REFERENCES

- [1] Bell, J.F. (1973). The Experimental Foundations of Solid Mechanics. *Encyclopedia of Physics*, Mechanics of Solids I, Vol. VIa/1, Eds. S. Flügge and C. Truesdell, Springer-Verlag, Berlin.
- [2] Cottrell, A.H. (1953). *Dislocations and Plastic Flow in Crystals*. University Press, Oxford.
- [3] Estrin, Y. and Kubin, L.P. (1995). Spatial coupling and propagative plastic instabilities. In *Continuum Models for Materials with Microstructures*, Ed. H.B. Mühlhaus, Wiley, New York, 395-453.
- [4] Hähner, P., Ziegenbein, A., Rizzi, E. and Neuhäuser, H. (2001). Spatio-temporal analysis of Portevin–Le Châtelier deformation bands: theory, simulation and experiment. Submitted.
- [5] Hähner, P. and Rizzi, E. (2001). On the kinematics of Portevin–Le Châtelier bands: theoretical and numerical modeling. Preprint.
- [6] Rizzi, E. and Hähner, P. (2001). On the Portevin Le-Châtelier effect: theoretical modeling and numerical results. Preprint.
- [7] Zaiser, M. and Hähner, P. (1997). Oscillatory modes of plastic deformation: theoretical concepts. *physica status solidi (b)*, 199, 267-330.

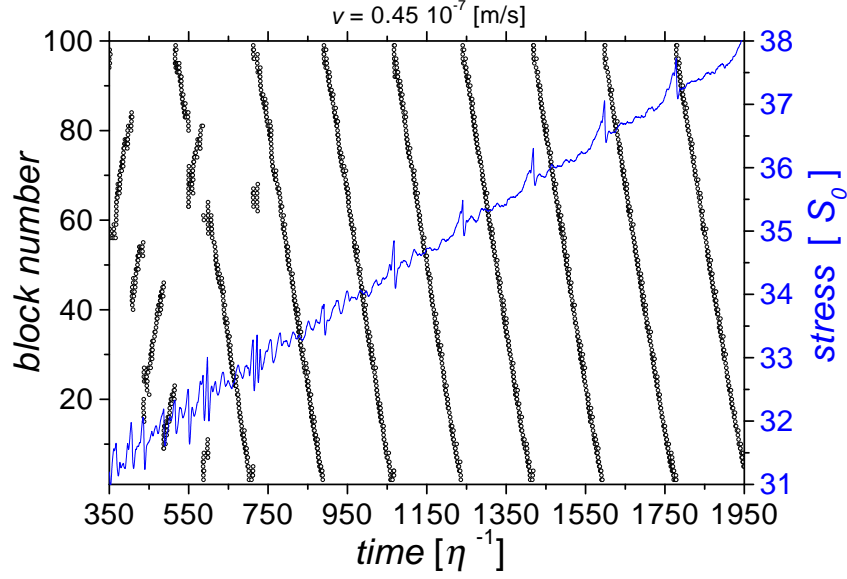


Figure 1: Uniaxial tension test simulated at constant applied cross-head velocity in the PLC range, $v=0.45 \cdot 10^{-7}$ m/s ($\eta=0.1$ s $^{-1}$, $S_0=1$ MPa): space–time localization map of plastic strain rate activity (left axis, scatter plot with circles) and corresponding stress–time curve (right axis, continuous line) in a time window showing Type C and Type B PLC bands.

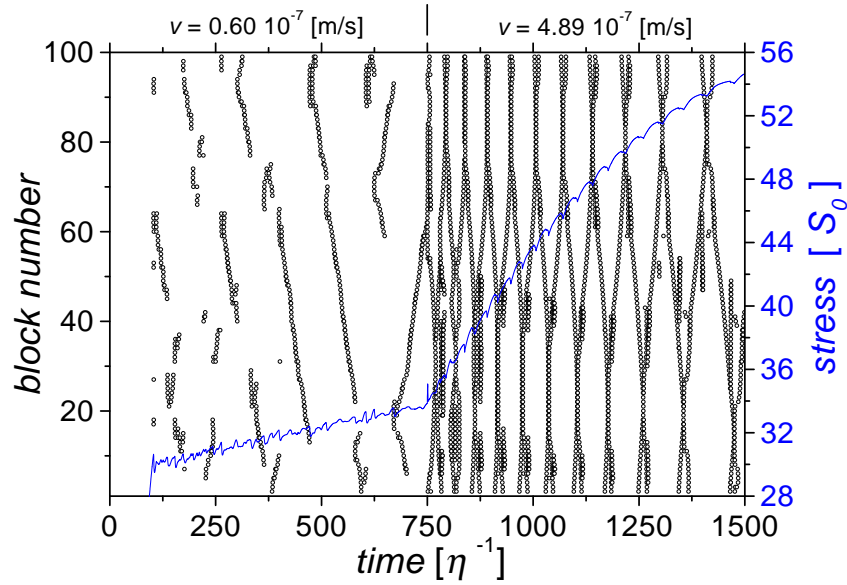


Figure 2: Uniaxial tension test simulated at constant applied cross-head velocities in the PLC range jumping from $v_0=0.60 \cdot 10^{-7}$ m/s to $v=3e v_0=4.89 \cdot 10^{-7}$ m/s ($\eta=0.1$ s $^{-1}$, $S_0=1$ MPa): space–time localization map of plastic strain rate activity (left axis, scatter plot with circles) and corresponding post-yield stress–time curve (right axis, continuous line) showing a sudden change of the PLC modes.

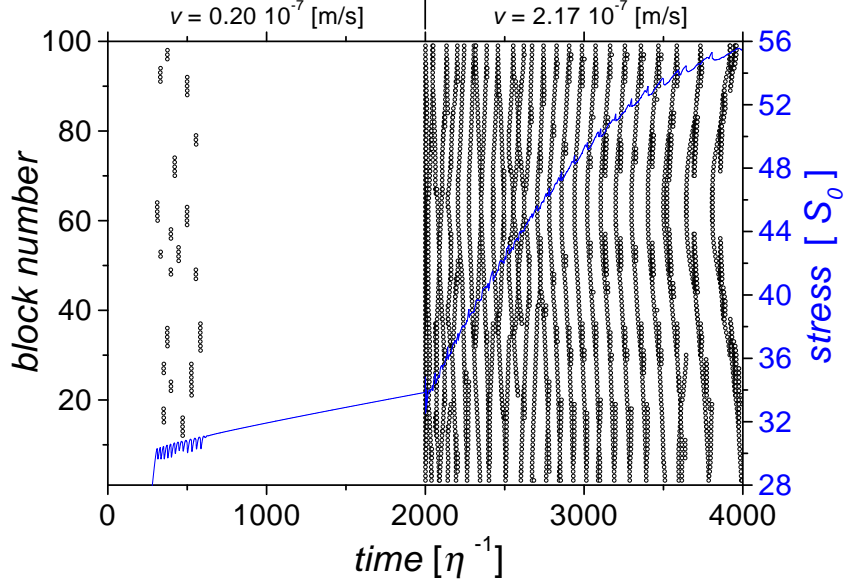


Figure 3: Uniaxial tension test simulated at constant applied cross-head velocities jumping into the PLC range from $v_0=0.20 \cdot 10^{-7}$ m/s to $v=4e v_0=2.17 \cdot 10^{-7}$ m/s ($\eta=0.1$ s $^{-1}$, $S_0=1$ MPa): space–time localization map of plastic strain rate activity (left axis, scatter plot with circles) and corresponding post-yield stress–time curve (right axis, continuous line) showing the sudden onset of the PLC effect.

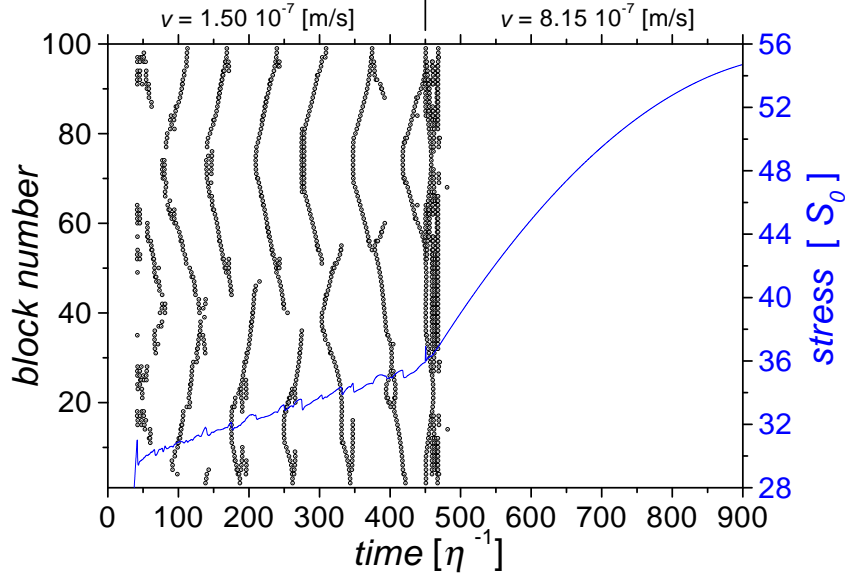


Figure 4: Uniaxial tension test simulated at constant applied cross-head velocities jumping outside the PLC range from $v_0=1.50 \cdot 10^{-7}$ m/s to $v=2e v_0=8.15 \cdot 10^{-7}$ m/s ($\eta=0.1$ s $^{-1}$, $S_0=1$ MPa): space–time localization map of plastic strain rate activity (left axis, scatter plot with circles) and corresponding post-yield stress–time curve (right axis, continuous line) showing the abrupt arrest of the PLC instability.

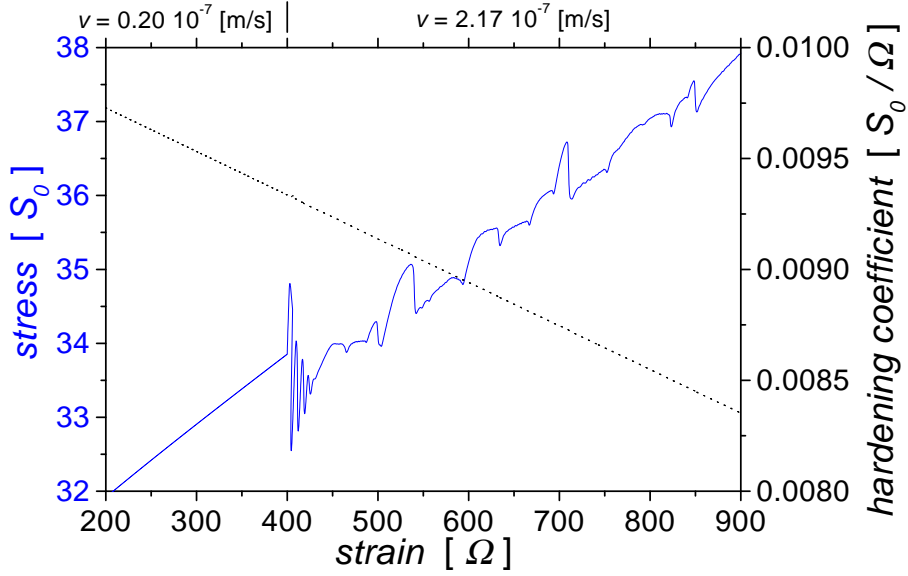


Figure 5: Uniaxial tension test simulated at constant applied cross-head velocities jumping into the PLC range from $v_0=0.20 \cdot 10^{-7}$ m/s to $v=4e v_0=2.17 \cdot 10^{-7}$ m/s ($\eta=0.1$ s $^{-1}$, $S_0=1$ MPa, $\Omega=10^{-5}$): stress–strain curve (left axis, continuous line) and imposed hardening coefficient θ (right axis, dotted line) in a window near the jump event (see also Fig. 3). The flow stress shows the positive instantaneous SRS S_0 and the negative asymptotic SRS S_∞ triggered by the jump into the PLC range.

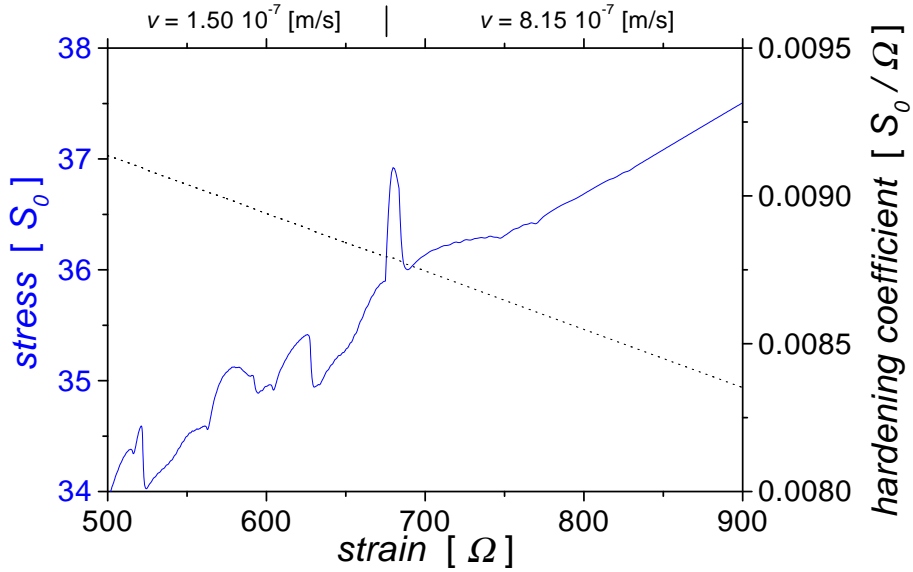


Figure 6: Uniaxial tension test simulated at constant applied cross-head velocities jumping outside the PLC range from $v_0=1.50 \cdot 10^{-7}$ m/s to $v=2e v_0=8.15 \cdot 10^{-7}$ m/s ($\eta=0.1$ s $^{-1}$, $S_0=1$ MPa, $\Omega=10^{-5}$): stress–strain curve (left axis, continuous line) and imposed hardening coefficient θ (right axis, dotted line) in a window near the jump event (see also Fig. 4). The flow stress shows the positive instantaneous SRS S_0 and the positive asymptotic SRS S_∞ consequent to the jump outside the PLC range.

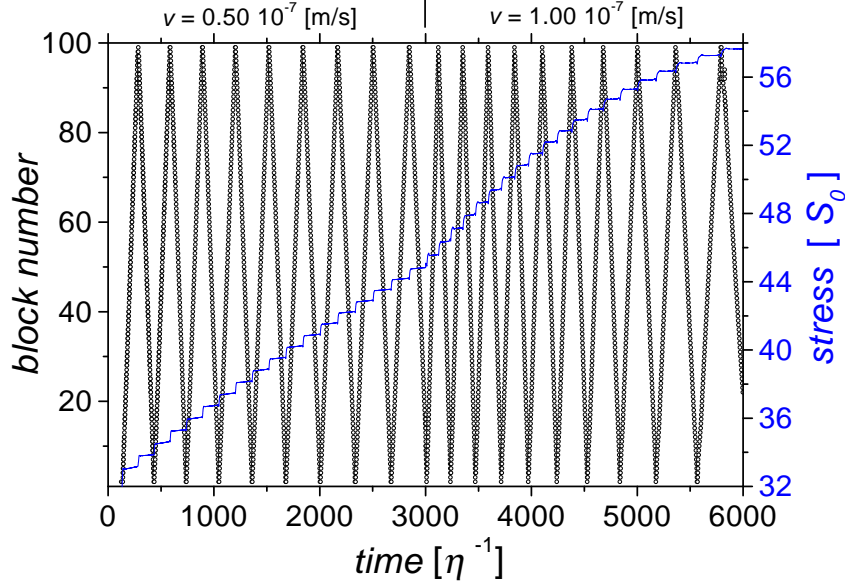


Figure 7: Uniaxial tension test simulated at constant applied cross-head velocities in the PLC range jumping from $v_0=0.50 \cdot 10^{-7}$ m/s to $v=2v_0=1.00 \cdot 10^{-7}$ m/s ($\eta=0.1$ s $^{-1}$, $S_0=1$ MPa): space–time localization map of plastic strain rate activity (left axis, scatter plot with circles) and corresponding post-yield stress–time curve (right axis, continuous line) showing reflective propagation of Type A PLC bands and the typical staircase profile of the stress trace.

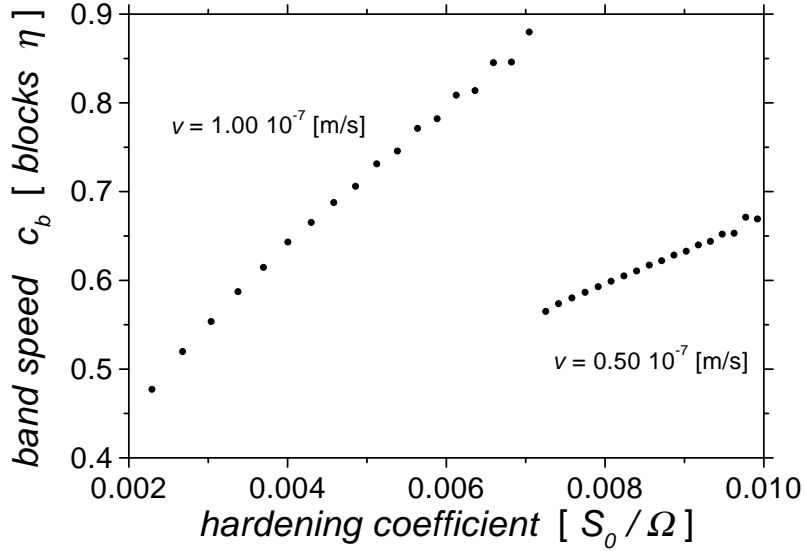


Figure 8: Same as Fig. 7 ($\eta=0.1$ s $^{-1}$, $S_0=1$ MPa, $\Omega=10^{-5}$). Characteristics of Type A PLC bands: band speed c_b as a function of hardening coefficient θ showing the sudden acceleration of the PLC band at the applied strain rate jump and a square root dependence on θ in agreement with eqn (6).

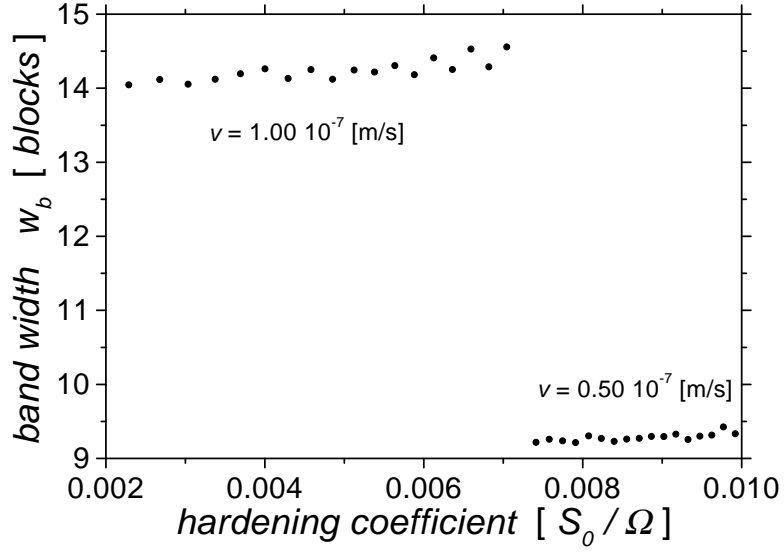


Figure 9: Same as Fig. 7 ($\eta=0.1 \text{ s}^{-1}$, $S_0=1 \text{ MPa}$, $\Omega=10^{-5}$). Characteristics of Type A PLC bands: band width w_b as a function of hardening coefficient θ showing the jump of the (nearly constant) band width in agreement with eqn (6).

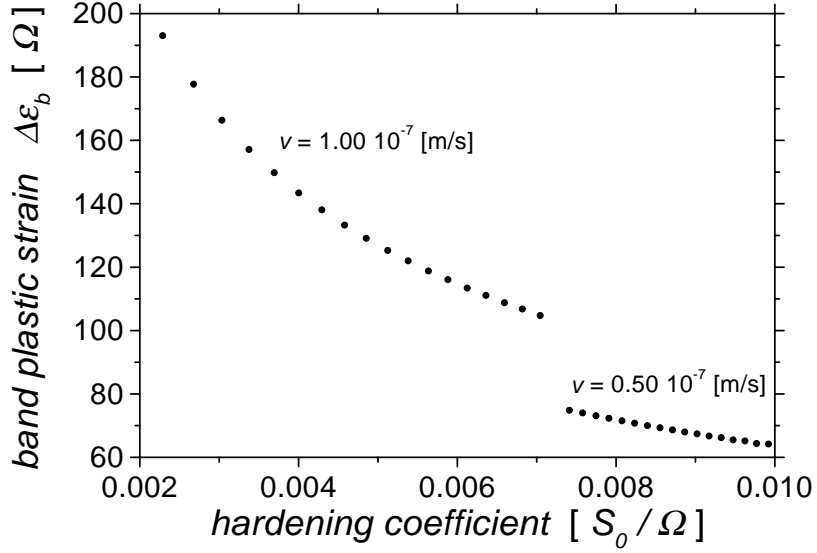


Figure 10: Same as Fig. 7 ($\eta=0.1 \text{ s}^{-1}$, $S_0=1 \text{ MPa}$, $\Omega=10^{-5}$). Characteristics of Type A PLC bands: band plastic strain $\Delta\epsilon_b$ as a function of hardening coefficient θ showing a jump consistent with the band width increase and an inverse square root dependence on θ in agreement with eqn (6).